

Structure and ferromagnetism properties of leaf-like ZnO nanostructures

Li Lijun ✉

Department of Electronic Engineering, Xi'an University of Posts and Telecommunications, Xi'an, Shaanxi 710121, People's Republic of China

✉ E-mail: lilijun007@163.com

Published in Micro & Nano Letters; Received on 5th April 2017; Revised on 5th August 2017; Accepted on 14th August 2017

Leaf-like macroscopic ZnO nanostructures have been synthesised via a conventional thermal evaporation method at 950°C, using a mixture of graphite, zinc oxide and CuO powders as a source material. The effect of CuO in a relevant growth mechanism was discussed. Its crystal structure properties were determined using X-ray diffraction, scanning electron microscopy and high resolution transmission electron microscopy. Photoluminescence spectra of the sample exhibit emission peaks centred at about 382, 525, 542 and 767 nm, respectively. The room temperature ferromagnetism was observed using a physical property measurement system.

1. Introduction: Being an important functional semiconductor material with a wide bandgap ($E_g = 3.37$ eV at 300 K) and a large exciton binding energy (60 meV), ZnO possesses many unique optical and electrical properties, such as high mechanical strength, excellent thermal stability, and chemical stability [1]. These properties make ZnO well suited for chemical sensors [2], ultraviolet laser arrays [3], cathode emitters of the field emission device [4], and so forth. Recently, exploring the wide bandgap diluted magnetic semiconductor (DMS) materials with room temperature ferromagnetism has attracted intense attention. ZnO has been considered as a promising candidate material for DMS, owing to its theoretically predicted and experimentally observed above room temperature ferromagnetism and long spin coherence time [5]. However, the origin and mechanism of the ferromagnetism in ZnO DMS are still controversial. In transition metal (TM)-doped ZnO, the origin of magnetism has been credited to the ferromagnetic coupling of the local moment of TM dopants through the carrier-mediated Ruderman–Kittel–Kasuya–Yosida interaction, indirect double exchange or super exchange [6]. Meanwhile, room temperature ferromagnetism has also been found in undoped ZnO and non-TM-doped ZnO [7, 8], and oxygen vacancies are deemed responsible for the observed ferromagnetism. It is interesting to research the ferromagnetism properties of these kinds of ZnO systems.

Low-dimensional oxide semiconductor materials usually exhibit a good degree of crystallisation, a high surface area-to-volume ratio, and a large number of deep energy level (DL) defects on the surface. High-quality ZnO nanostructures may be a good platform to research the origin of ferromagnetism in undoped and non-TM-doped ZnO. Low-dimensional ZnO nanostructures have been synthesised by a variety of methods, and thermal evaporation is the most common one. Various morphological features of ZnO nanostructures have been successfully studied using this method, such as nanowires, nanobelts, nanorods, and ‘ultra-long (centimetre long)’ ZnO nanostructures including nanocombs and hierarchical ZnO dendrites [9–12]. The source material used in the growth process is an important reason to impact the morphology of the product. Exploring the growth mechanism of ZnO nanostructures is still a challenging work.

In this Letter, leaf-like ZnO nanostructures were fabricated using a conventional thermal evaporation method with CuO as the source material. The relevant growth mechanism was discussed. Room temperature ferromagnetism was observed in the ZnO system, and the products consist of only non-magnetic elements.

2. Experiments: The growth was performed in a conventional horizontal quartz tube furnace with a length of 150 cm and a

diameter of 8 cm at atmospheric pressure. The source material used in the growth process was a uniform mixture of ZnO powder (99.99%, in purity), graphite powder (99%, in purity) and CuO powder (99.9%, in purity) with a mass ratio of 5:1:5. The tube furnace was heated to 950°C, and then argon (99.99%, in purity) was introduced into the tube as a carrier gas at a flow rate of 800 sccm. Ten minutes later, a quartz boat loaded with source materials and a piece of single-crystal silicon substrate 5 mm away from the source was pushed into the centre of the tube. After the growth process (about 1.5 h), the furnace was cooled down to room temperature under the same argon gas flow. Finally, a quantity of white semi-transparent crystal material was found on the silicon substrate surface of the reactant powder.

The obtained sample was investigated by X-ray diffraction (XRD), scanning electron microscopy (SEM), high-resolution transmission electron microscopy (HRTEM), selected area electron diffraction (SAED) and photoluminescence (PL) spectra. The magnetic properties were determined using a physical property measurement system (PPMS) at 300 and 5 K.

3. Results and discussion: XRD was employed to confirm the crystalline structure of the as-fabricated ZnO nanostructures as shown in Fig. 1. The diffraction peaks indicated that the products are the hexagonal phase (wurtzite structure) of ZnO with lattice constants of $a = b = 0.325$ nm and $c = 0.521$ nm, which correspond with the data of ZnO powder recorded in the JCPDS document (Powder Diffraction File Compiled by the Joint Committee on Powder Diffraction, 1985, JCPDS Card No. 80-0074). All the sharp diffraction peaks at around 31.6°, 34.4°, 36.3°, 47.7°, 56.8°, 63.1° and 68.2° fit well with the (100), (002), (101), (102), (110), (103) and (112) crystal planes of ZnO, respectively. No peaks of copper or other impurities were observed within the sensitivity of XRD measurements.

The morphologies of as-fabricated ZnO products were examined by SEM. Leaf-shaped crystal materials covered most of the substrates, Fig. 2a clearly shows a typical leaf-like ZnO nanostructure. In the middle of the leaf is the major vein, with a length of nearly 600 µm, a diameter of nearly 2 µm, and highly ordered lateral veins on both sides of the major vein. The lateral veins are parallel to each other, with a length of nearly 200–300 µm, a diameter of several hundred nanometres, and emerge at the same angles with respect to the major vein. From further observation of the lateral veins as shown in Fig. 2b, they are composed of secondary branches with length of nearly 10 µm, diameters of several hundred nanometres, and difference in the orientation, present a three-dimensional netted venation structure.

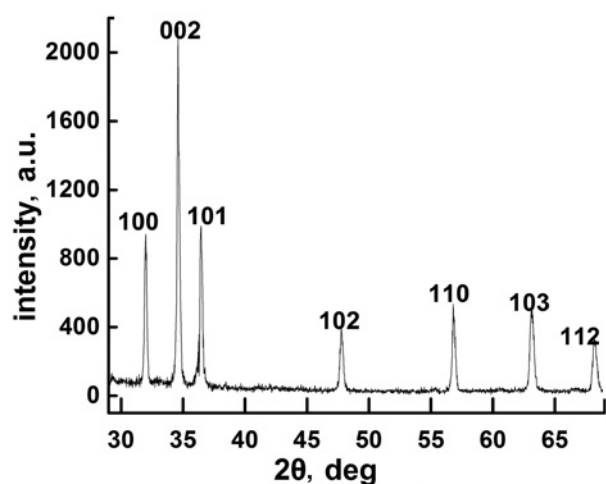


Fig. 1 XRD pattern of the as-fabricated ZnO sample

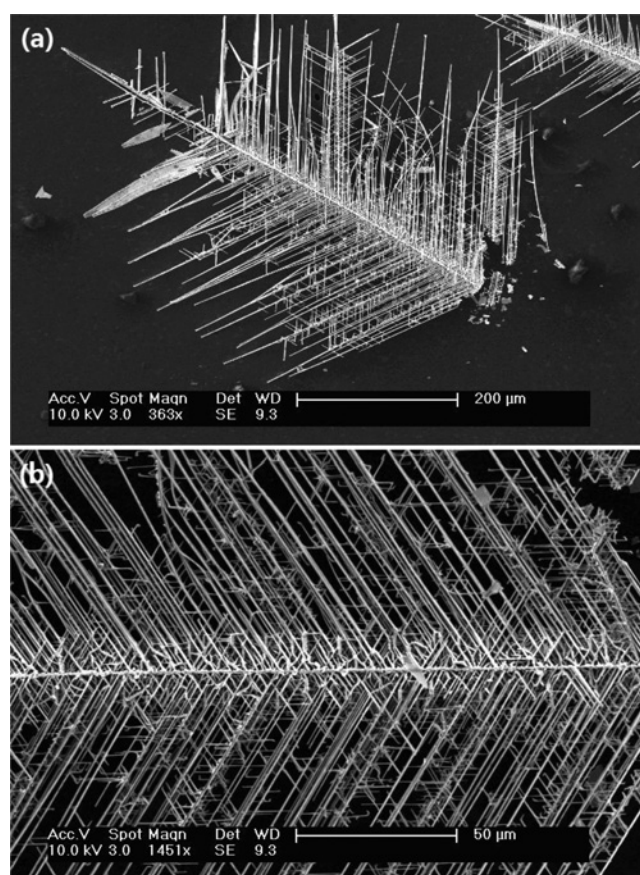


Fig. 2 SEM image of the as-fabricated ZnO sample

a SEM image of a typical leaf-like ZnO structure
b High magnification SEM image of the centre of the leaf-like ZnO shown in a

HRTEM and SAED were used to in-depth study the crystal structure and formation mechanism of the sample. The transmission electron microscopy (TEM) image of leaf-like ZnO with a width of nearly 1.5 μm is shown in Fig. 3a, inset is the SAED pattern. The HRTEM images of the major and lateral veins indicated by the red dotted line rectangles 1 and 2 are shown in Figs. 3b and c. It is indicated that both the major and lateral veins of the leaf-like sample exhibit single-crystalline nature, and grow along [10–13] and [0001] directions, respectively. Figs. 3d and e are the

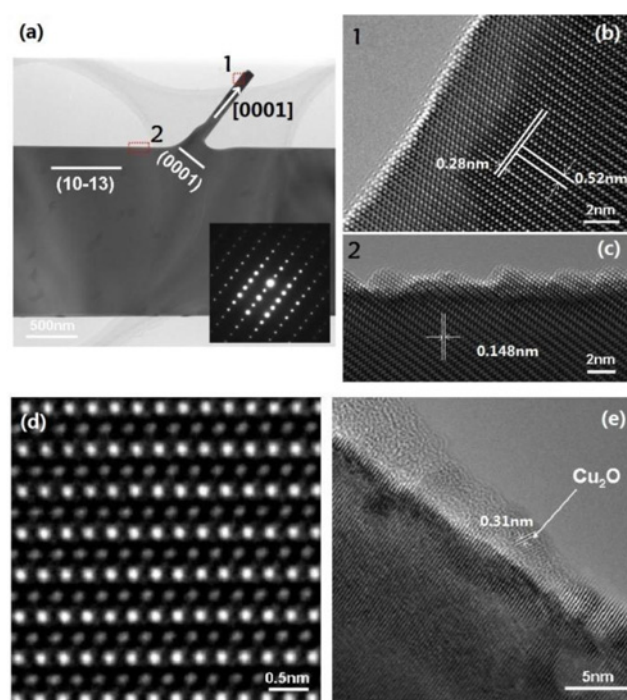


Fig. 3 TEM image of the as-fabricated ZnO sample

a TEM image of the as-fabricated ZnO, inset shows the SAED pattern
b, c HRTEM images of the marked 1 and 2 parts in a
d HRTEM image of the inner part of the as-fabricated ZnO
e HRTEM image of the edge part of the as-fabricated ZnO

HRTEM images of an arbitrary point from the inner and edge of the sample. It can be observed that the internal lattice structure of the sample is complete without defects, but a small amount of Cu_2O nanoparticles was distributed on the edge of the vein. In our experiments, CuO powder was added into the reactant mixture powder, which was supposed to play a critical role in the formation of leaf-like ZnO. It can be concluded that the growth of the product follows the classical vapour–liquid–solid mechanism. Cu ions retain the liquate droplet in the process of growth and finally rest on the surface.

Normally, the preferential growth direction of ZnO is [0001], and then [10–10] and [0110] directions [13]. When the source material was a mixture of graphite and ZnO powder, first the reduced Zn vapour cooled down to Zn liquid on the substrates, and then combined with O to produce a large number of ZnO crystal nuclei after the concentration of Zn and O elements reached super saturation, finally a large number of ZnO nanocrystals were synthesised. The typical ZnO nanowires and nanoribbons [14] were synthesised by the method. In our experiments, CuO was added into the source materials (a mixture of graphite and ZnO powders), which is supposed to play a critical role in the formation of micron or millimetre size leaf-like ZnO samples. At high temperatures, carbon thermal reduction reaction occurred, CuO and ZnO powders were reduced to metal Cu and Zn particles. Next, the Zn atoms would dissolve in Cu particles to form a Cu–Zn eutectic phase, because Zn is largely soluble in the Cu solid solution according to the Cu–Zn binary phase diagram. Then Cu–Zn eutectic reacted with oxygen originating from the residual oxygen in the quartz tube to form liquid droplets of the Zn–Cu–O eutectic phase. The precipitation rate of ZnO nuclei became slow because the solubility of Zn in the Zn–Cu–O eutectic was large and the corresponding super saturation degree of Zn was lower. Meanwhile, Zn vapour was evenly generated in a stable and durable manner and the effective reaction time was obviously increased. The density of ZnO crystal nucleus was therefore significantly reduced and every crystal nucleus could grow to larger size crystal structures compared with the

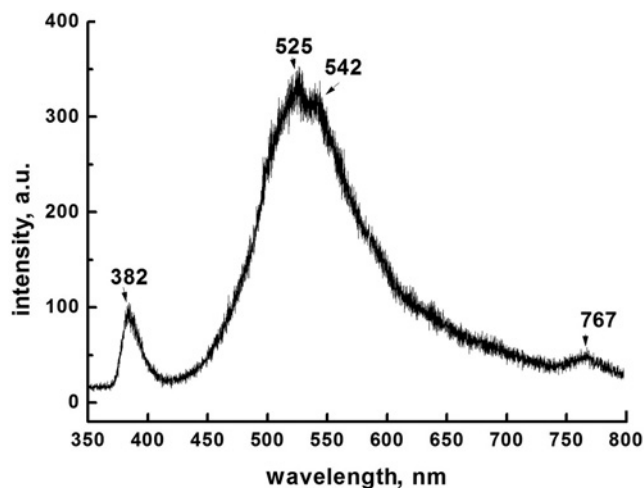


Fig. 4 PL spectra of the as-fabricated ZnO sample

situation without added CuO powder. In addition, the growth rate along the [0001] direction was limited by the insufficient Zn source; meanwhile the relative speed along the [10-13] direction became faster in the initial stage of nucleus formation. So the major vein of leaf-like ZnO formed. As the reaction proceeds, the percentage of Zn in the Zn-Cu-O eutectic increased persistently. As the preferential growth direction of ZnO was [0001] as usual, so the lateral veins grew rapidly. At the same time, the residual Cu adheres to the surface of the ZnO crystal in the form of Cu₂O nanoparticles. Finally, leaf-like macroscopic size ZnO crystal structures with a small quantity of Cu₂O nanoparticles on the surface would be achieved.

Fig. 4 shows the PL spectra measured from 350 to 800 nm using a 325 nm He-Cd laser. The sample exhibits four obvious luminescence peaks: an ultraviolet emission peak centred at about 382 nm, a green emission peak at around 525 nm with a shoulder peak at 542 nm, and a feeble red emission peak at about 767 nm. The energy of peak centred at 382 nm is 3.246 eV, a little less than the energy gap of ZnO (3.37 eV), could be explained by the near-band edge (NBE) emission and is in good agreement with the typically reported free exciton radiative recombination luminescence. It has been generally believed that the green emission of ZnO is the DL emission originates from oxygen vacancies [15, 16]. Therefore, the peaks at 525 and 542 nm are results from the radiative recombination of a photo-generated hole with an electron occupying the oxygen vacancy. The peak around 767 nm may be due to Cu₂O nanoparticles, which is seldom observed in ZnO PL spectra. The intensity ratio of luminescence peaks from the NBE and DL emissions of as-synthesised ZnO is about 1:4, indicated that the crystal quality is good and a sufficient quantity of DL defects existed in the sample.

The magnetic properties of leaf-like ZnO were determined by using the PPMS. Fig. 5a shows the curves of magnetisation to a magnetic field of the as-prepared leaf-like ZnO at 5 and 300 K. The as-prepared ZnO has a saturation magnetisation of ~0.0062 emu/g at 5 K, and decreased to ~0.0038 emu/g at 300 K. The hysteresis loop clearly indicates that the ferromagnetism of ZnO is robust even above the room temperature. A magnetisation to temperature curve as shown in Fig. 5b was measured under a magnetic field of 5 kOe under zero field-cooled conditions. The magnetisation decreases obviously from 5 to 100 K, without blocking or spin-glass shape in the whole curve.

Magnetic secondary phases are not responsible for the observed ferromagnetism because no such phases exist in the system. It can be confirmed that the leaf-like ZnO sample is a pure single-crystal ZnO structure and a few Cu₂O nanoparticles existed on the surface. Cu atoms in a unionised state have an outer cell electronic

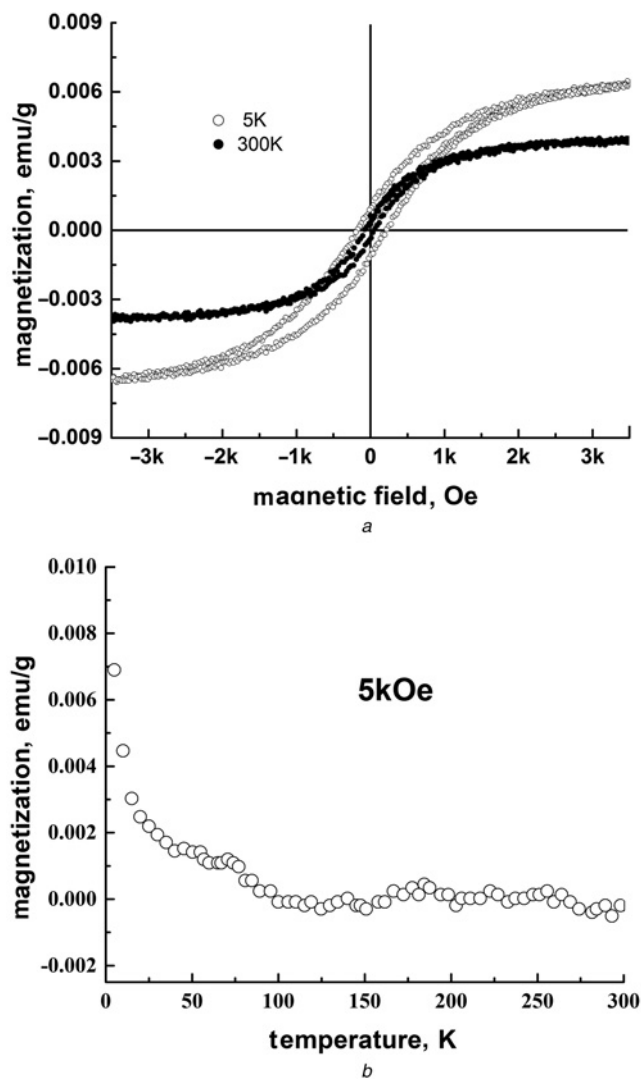


Fig. 5 The magnetic properties of the as-fabricated ZnO sample
a Magnetisation to a magnetic field curve of the as-fabricated ZnO sample measured at 5 K (hollow circle) and 300 K (solid circle)
b Magnetisation to the temperature curve of the as-fabricated ZnO sample

configuration of 3d¹⁰4s¹ and Cu⁺ ions are expected to possess 3d¹⁰ configurations, in which, all the d electrons are paired, hence a Cu⁺ ion does not possess any magnetic moment. Cu⁺ may contribute less to the observed room temperature ferromagnetisms in our samples. The room temperature ferromagnetic ordering in Cu-doped ZnO samples has been reported both in theoretical and experimental sides [8, 17]. However, no evidence indicated the presence or absence of Cu²⁺ in the sample within the sensitivity of the used measurements. The origin of the ferromagnetism in pure oxides such as ZnO was attributed to the vacancies in the lattice [18], as well as in other oxides such as SnO₂ and TiO₂ have already been indicated [19, 20]. The PL result shows that a sufficient quantity of DL defects existed in the sample. The high surface area-to-volume ratio for the structures favours a higher concentration of vacancies in the surface, which result in the ferromagnetism. Further study is undergoing to interpret the origin of the ferromagnetism of ZnO.

4. Conclusion: In summary, a leaf-like macroscopic ZnO nanostructure has been successfully fabricated via a thermal evaporation method. CuO played a critical role in the formation of as-fabricated ZnO samples. The PL spectra of the sample exhibited emission peaks centred at about 382, 525, 542 and 767 nm,

respectively. The low-intensity ratio of luminescence peaks from NBE and DL emissions indicated that a sufficient quantity of DL defects existed in the sample due to oxygen vacancies. Vacancies on the surface were responsible for the observed room temperature ferromagnetism of the leaf-like ZnO nanostructure.

5. Acknowledgments: This work was supported by the Scientific Research Program Funded by Shaanxi Provincial Education Department (grant no. 14JK1656).

6 References

- [1] Wang Z.L., Kong X.Y., Ding Y., *ET AL.*: 'Semiconducting and piezoelectric oxide nanostructures induced by polar surfaces', *Adv. Funct. Mater.*, 2004, **14**, (10), pp. 943–956
- [2] Mani G.K., Bosco J., Rayappan B.: 'ZnO nanoarchitectures: ultrahigh sensitive room temperature acetaldehyde sensor', *Sens. Actuators B, Chem.*, 2016, **223**, (6), pp. 343–351
- [3] Yan H., He R., Johnson J., *ET AL.*: 'Dendritic nanowire ultraviolet laser array', *J. Am. Chem. Soc.*, 2003, **125**, (16), pp. 4728–4729
- [4] Chen S., Chen J.T., Liu J.L., *ET AL.*: 'The effect of high temperature oxygen annealing on field emission from ZnO nanowire arrays', *Appl. Surf. Sci.*, 2015, **357**, pp. 413–416
- [5] Yang Z.: 'A perspective of recent progress in ZnO diluted magnetic semiconductors', *Appl. Phys. A*, 2013, **112**, (2), pp. 241–254
- [6] Bruno P., Chappert C.: 'Oscillatory coupling between ferromagnetic layers separated by a nonmagnetic metal spacer', *Phys. Rev. Lett.*, 1991, **67**, p. 1602
- [7] Panigrahy B., Aslam M., Misra D.S., *ET AL.*: 'Defect-related emissions and magnetization properties of ZnO nanorods', *Adv. Funct. Mater.*, 2010, **20**, (7), pp. 1161–1165
- [8] Kumar S., Thangavel R.: 'Structural, optical and magnetic characterization of ZnO nanorods synthesized using hydrothermal technique at low temperature', *J. Sol-Gel Sci. Technol.*, 2014, **70**, (3), pp. 506–510
- [9] Morales A.M., Lieber C.M.: 'A laser ablation method for the synthesis of crystalline semiconductor nanowires', *Science*, 1998, **279**, (5348), pp. 208–211
- [10] Yang P.D., Lieber C.M.: 'Nanostructured high-temperature superconductors: creation of strong-pinning columnar defects in nanorod/superconductor composites', *J. Mater. Res.*, 1997, **12**, (11), pp. 2981–2996
- [11] Pan Z.W., Dai Z.R., Wang Z.L.: 'Nanobelts of semiconducting oxides', *Science*, 2001, **291**, (5510), pp. 1947–1949
- [12] Yu K., Zhang Q.X., Wu J., *ET AL.*: 'Growth and optical applications of centimeter-long ZnO nanocombs', *Nano Res.*, 2008, **1**, (3), pp. 221–228
- [13] Wang Z.L.: 'Nanostructure of zinc oxide', *Mater. Today*, 2004, **7**, (6), pp. 26–33
- [14] Yao B.D., Chan Y.F., Wang N.: 'Formation of ZnO nanostructures by a simple way of thermal evaporation', *Appl. Phys. Lett.*, 2002, **81**, (4), pp. 757–759
- [15] Kohan A.F., Ceder G., Morgan D., *ET AL.*: 'First-principles study of native point defects in ZnO', *Phys. Rev. B*, 2000, **61**, (22), pp. 15019–15027
- [16] Xing G.Z., Yi J.B., Tao J.G., *ET AL.*: 'Comparative study of room-temperature ferromagnetism in Cu-doped ZnO nanowires enhanced by structural inhomogeneity', *Adv. Mater.*, 2008, **20**, (18), pp. 3521–3527
- [17] Ye L.H., Freeman A.J., Delley B.: 'Half-metallic ferromagnetism in Cu-doped ZnO: density functional calculations', *Phys. Rev. B*, 2006, **73**, (3), Article id 033203
- [18] Banerjee S., Mandal M., Gayathri N., *ET AL.*: 'Enhancement of ferromagnetism upon thermal annealing in pure ZnO', *Appl. Phys. Lett.*, 2007, **91**, (18), Article id 182501
- [19] Sundaresan A., Bhargavi R., Rangarajan N., *ET AL.*: 'Ferromagnetism as a universal feature of nanoparticles of the otherwise nonmagnetic oxides', *Phys. Rev. B*, 2006, **74**, (16), Article id 161306
- [20] Hong N.H., Sakai J., Poirot N., *ET AL.*: 'Room-temperature ferromagnetism observed in undoped semiconducting and insulating oxide thin films', *Phys. Rev. B*, 2006, **73**, (13), Article id 132404